Probing Hydrogen Bond Strength in Liquid Water by Resonant inelastic X-ray scattering

Vinícius Vaz da Cruz[1*], Faris Gel'mukhanov[1,2], Sebastian Eckert[3], Marcella Iannuzzi[4], Emelie Ertan[5], Annette Pietzsch[6], Rafael C. Couto[1], Johannes Niskanen[7,6], Mattis Fondell[6], Marcus Dantz[8], Thorsten Schmitt[8], Xingye Lu[8], Daniel McNally[8], Raphael M. Jay[3], Victor Kimberg[1,2], Alexander Föhlisch[3,6] & Michael Odelius[5*]

[1]*Theoretical Chemistry and Biology, Royal Institute of Technology, 10691 Stockholm, Sweden*

[2]*Laboratory for Nonlinear Optics and Spectroscopy, Siberian Federal University, 660041 Krasnoyarsk, Russia*

[3]*Institut für Physik und Astronomie, Universität Potsdam, Karl-Liebknecht-Strasse 24-25, 14476 Potsdam, Germany*

[4]*Physical Chemistry Institute, University of Zürich, 8057 Zürich, Switzerland*

[5]*Department of Physics, Stockholm University, AlbaNova University Center, 10691 Stockholm Sweden*

[6]*Institute for Methods and Instrumentation in Synchrotron Radiation Research FG-ISRR, Helmholtz-Zentrum Berlin für Materialien und Energie Albert-Einstein-Strasse 15, 12489 Berlin, Germany*

[7]*Department of Physics and Astronomy, University of Turku, FI-20014, Turun yliopisto, Finland*

[8]*Research Department Synchrotron Radiation and Nanotechnology, Paul Scherrer Institut, CH-5232 Villigen PSI, Switzerland; e-mail * vvdc@kth.se, odelius@fysik.su.se*

Local probes of the ground state potential are essential for understanding hydrogen bonding in aqueous environments, which influences a vast array of processes in chemistry, biology and atmospheric science. When tuned to the dissociative core-excited state at the O$1s$ pre-edge, resonant inelastic X-ray scattering (RIXS) back to the electronic ground state exhibits a long vibrational progression due to ultrafast nuclear dynamics[1–3]. We show here how the coherent evolution of the OH bonds around the core-excited oxygen provides access to high vibrational levels in liquid water. The OH bonds stretch into the long range part of the potential energy curve (PEC), which makes RIXS more sensitive than IR spectroscopy to the local environment. We exploit this property to effectively probe hydrogen bond (HB) strength via the distribution of intramolecular OH PECs extracted from RIXS measurements. Establishing how sensitive the RIXS spectrum is to HB rearrangements, and the underlying structural implications, is a hotly debated[2,4–9] issue. There have also been attempts[2,4–9] to investigate the local structure in liquid water using the RIXS channel, in which the decay transition happens between the non-bonding $1b_1$ lone-pair and the $1s_O$ core-hole. However, we show here that the splitting emerging for pre-edge core-excitation has a purely dynamical origin and is primarily sensitive to the short range part of the PEC since the splitting is formed at short time-scales before fragmentation. Thereby, we establish how RIXS spectroscopy can be used as a structural probe in aqueous solution[2,4–9].

There are competing conceptions of the local structure of liquid water; Either as a continuum of different H-bonding configurations[10–12], or as a mixture of two structural motives[4,9]. For enhanced insight, we derive the distribution of PECs of OH bonds with broken and intact HBs as reconstructed

from experimental RIXS data. The method of reconstruction is inspired by the observed breakdown of the one-to-one correspondence between RIXS peak positions and vibrational quantum numbers[1,2]. The suggested approach is based on a solid theoretical foundation composed of classical *ab initio* MD simulations, calculation of local potential energy surfaces from the sampled configurations, and quantum wave packet modelling of the nuclear motion in relevant degrees of freedom.

Vibrationally resolved RIXS measurements of gas phase and liquid water, presented here (Fig. 1), were performed at the Swiss Light Source[13] (see Methods). The photon frequency ω was tuned near resonance with the lowest core-excited state and the decay back to the ground electronic state was studied. In gas phase, core-excitation to the $|O1s^{-1}4a_1^1\rangle$ state leads to ultra-fast dissociation along the OH bonds[3,14,15]. The propagation of the nuclear wave packet[3,14,15] results in the long vibrational progression seen in both theory and experiment. In the liquid, however, we observe a strong shortening of the vibrational progression in comparison to the gas phase (Fig. 1 (a) and (b)). Our simulations show that this shortening arise from fluctuations in the OH PECs, reflecting the local HB environments (Fig. 1 (c)). These fluctuations affect mainly the long range part of the OH PEC and result in a variation of the high vibrational levels, seen in the partial density of vibrational states of the n-th group $\rho_n(\epsilon)$ (see Fig. 1 (d) and Methods) . Each groups is characterised by the group number $n = n_1 + n_2$[3], where n_1 and n_2 are the vibrational quantum numbers for the stretching modes along the OH bonds (see Methods). In Fig. 1 (d), we notice for $n \geq 2$ a strong overlap of the partial density of states ρ_n belonging to different groups. Hence, the adjacent density of states $\rho_{m-1}(\epsilon)$ and $\rho_{m+1}(\epsilon)$ can contribute to the m-th peak. The high-energy part of the spectrum ($\gtrsim 3$ eV) is smeared (Fig. 1 (a) and (b)) by fluctuations in local environment

into a smooth background (Fig. 1 (e)). Thus ρ_n qualitatively explains the shortening of the spectrum and the increasing peak width (see insert in Fig. 1 (b)). Because of the shared core-excitation, the OH bonds are coherently excited in RIXS, as illustrated by the nuclear wave packet in Fig. 2 (a), also in asymmetric environments. Our *ab-initio* RIXS analysis does not support previous empirical analyses of single bonds[1] (dashed line in Fig. 2c) or of normal modes[2].

It has been argued that the X-ray spectra are sensitive to the local structure of the liquid water[4,9–11,16]. We investigated the sensitivity of RIXS to hydrogen bonding based on the classification of "double-donor" (D2) and "single-donor" (D1) structures, in which either both OH groups in the water molecule donate a hydrogen bond, or just one OH group (see Methods). The pre-edge region in the X-ray absorption spectrum (XAS) of liquid water has been ascribed to excitation of molecules in asymmetric HB environments (D1), where the assumed selectivity depends on the XAS simulation method[16–19]. The employed excited core-hole (XCH) approximation[18,20] yields enhanced transitions dipole moments for D1 structures. Hence, the partial RIXS cross sections σ_{D1} and σ_{D2} in Fig. 2 (b) contribute almost equally to the RIXS profile, even though the D1 structures are in minority (only 20%) in our MD simulation (see Methods). The progression in σ_{D2} is red-shifted with respect to σ_{D1}, since the D2 structures on average experience shallower potentials than the D1 structures. This red-shift together with their intrinsic spread allow us to explain the formation of a background in the total profile $\sigma = \sigma_{D1} + \sigma_{D2}$ (see Fig. 1 (e) and Fig. 2 (d)).

The simulated RIXS spectrum of an individual D1 configuration (Fig. 2 (d)) differs very much from the one in gas-phase (Fig. 1). The asymmetric environment leads to a complicated spectrum

formed by single bond excitations ((n_1,0) and (0,n_2)) and mixed bond excitations (n_1, n_2). We see from Fig. 2 (e) that the eigenvalues of the steep potential (weak HB) approximately match the peak positions of the total sampled RIXS spectrum in contrast to the shallow potential (strong HB) which shows considerable deviations as even two eigenvalues may belong to the same peak (Fig. 2 (d)). Neglecting this effect we obtain an artificially narrow distribution of OH potentials (see below and Fig. 3 (a)) not capturing the broad distribution of the OH PECs of liquid water seen in Fig. 2 (e).

Thus, a key insight from the simulations is that to extract potential information, we need to design a method that allows for more than one vibrational eigenvalue to be located within the energy range around a given m-th peak in the observed RIXS progression. In a conservative attempt to estimate the confidence interval, we define this energy range $\Delta\varepsilon_m$ as the spacing between two adjacent minima of this peak and introduce the distribution of the number of vibrational eigenvalues per peak ordered according to the peak's number (123456). For example

$$\text{weak or no HB} \qquad (111111), \quad (111112), \tag{1}$$

$$\text{strong HB} \qquad (112212), \quad (112222), \cdots \tag{2}$$

Our simulations show that no more than two vibrational eigenstates can belong to a given peak in the spectrum. The variation of the local environment leads to a variation in the eigenvalue distribution, which depends on the shape of the OH PEC: There is only one vibrational level within each peak for the steep potentials (weak or no- HB), the only exception being the peaks with $m \geq 6$ (see eq. (1) and Fig. 2 (d)). In contrast, two vibrational levels of a shallow potential (HB) can lie within

the m-th peak, except for $m = 1$ (see eq. (2) and Fig. 2 (d)). Since the eigenvalues belonging to the m-th peak are only confined to a $\Delta\varepsilon_m$ interval, the constraints (Eqs. (1) and (2)) generate a distribution of PECs which defines the confidence interval of the OH potentials. To extract the confidence interval we designed a procedure (see Methods) using a genetic algorithm[21] which was validated for the theoretical RIXS spectrum of liquid water (Fig. 1 (a)) and then applied to the experimental RIXS spectrum (Fig. 1 (b)) to extract a distribution of PECs in liquid water with a minimal model dependence. The constraint given by eq. (1) alone results in a narrow confidence interval (Fig. 3 (a)) which is associated solely with the OH potentials weakly affected by HB (steep potentials). In contrast, the constraint defined in eq. (2) results in a much wider distribution (Fig. 3 (b)) related to various HB configurations. The total reconstructed confidence interval (Fig. 3 (c)) comprises both narrow and shallow PECs. Thus, in spite of the inherent chaotic nature of liquid water, RIXS data provides the possibility to, within confidence intervals, separately determine PECs for OH groups involved in weak and strong HBs.

The local HB enviroment has also been probed in electronically inelastic processes[2,4–9]; Decay channels in which the $1s_O$ core hole is filled by a transition from the occupied lone-pair orbital $1b_1$. This transition forms a split peak (Fig. 4) which has been attributed either to two distinct ground state structural motifs[4,9] or to nuclear motion after core excitation[2,5–8]. Here, we investigate the very onset of the splitting by looking at the evolution of the RIXS spectrum as a function of detuning Ω, from below the pre-edge into the main edge of XAS. The extend of nuclear dynamics can be controlled via the effective scattering duration[22] $\tau = 1/\sqrt{\Omega^2 + \Gamma^2}$, which monotonously approaches $\Gamma^{-1} = 8$ fs from <1 fs.

The experimental RIXS spectra shown in Fig. 4 display the striking quantitative coincidence of the ω-dependence of the $1b_1$ splitting in liquid and gas phases. This indicates the same dynamical origin of the splitting as recently established for the gas phase[15] associated with the different dispersion laws of the pseudo-atomic and molecular peaks. The pseudo-atomic peak is formed due to the similar non-bonding characters of $1s_O$ and lone-pair $1b_1$ orbitals which make the potential surfaces of core-excited and final states almost parallel already at moderate distortions (see Fig. 4 (e)). Since both molecular and pseudo-atomic $1b_1$ peaks arise from decay near the equilibrium, the splitting is insensitive to HB fluctuations[6]. Environment-dependent fluctuations in emission energy near equilibrium can be characterised by a distribution function $\rho(\omega_1' - \omega')$. We can reconstruct the liquid spectrum $\sigma_{\mathrm{liquid}}(\omega', \omega)$ by convolution of the experimental gas-phase spectrum $\sigma_{\mathrm{gas}}(\omega', \omega)$ with $\rho(\omega_1' - \omega')$ (see Methods). In Fig. 4, the reconstructed spectrum $\sigma_{\mathrm{liquid}}(\omega', \omega)$ is shown to be in good agreement with the experimental spectrum of liquid water.

In conclusion, we show that both OH bonds are coherently excited in RIXS, also for hydrated water molecules. Fluctuation of the OH potentials with strong HB results in a shortening of the vibrational progression of RIXS in liquid water. The PECs for OH bonds with weak and strong HB are derived from RIXS to characterise HB strength. We show that the lone-pair ($1b_1$) peak splitting is of dynamical origin, corroborating previous experimental observations of the large isotope effect on the $1b_1$ peak[5,8] and contradicting a structural interpretation[4,9] of the splitting.

1. Harada, Y. *et al.* Selective probing of the OH or OD stretch vibration in liquid water using resonant inelastic soft-x-ray scattering. *Phys. Rev. Lett.* **111**, 193001 (2013).

2. Pietzsch, A. *et al.* Snapshots of the fluctuating hydrogen bond network in liquid water on the sub-femtosecond timescale with vibrational resonant inelastic x-ray scattering. *Phys. Rev. Lett.* **114**, 088302 (2015).

3. Couto, R. C. *et al.* Selective gating to vibrational modes through resonant x-ray scattering. *Nat. Commun.* **8**, 14165 (2017).

4. Tokushima, T. *et al.* High resolution X-ray emission spectroscopy of liquid water: The observation of two structural motifs. *Chem. Phys. Lett.* **460**, 387–400 (2008).

5. Fuchs, O. *et al.* Isotope and Temperature Effects in Liquid Water Probed by X-Ray Absorption and Resonant X-Ray Emission Spectroscopy. *Phys. Rev. Lett.* **100**, 027801 (2008).

6. Odelius, M. Molecular dynamics simulations of fine structure in oxygen k-edge x-ray emission spectra of liquid water and ice. *Phys. Rev. B* **79**, 144204 (2009).

7. Odelius, M. Information content in o[1s] k-edge x-ray emission spectroscopy of liquid water. *J. Phys. Chem. A* **113**, 8176–8181 (2009).

8. Weinhardt, L. *et al.* Nuclear dynamics and spectator effects in resonant inelastic soft x-ray scattering of gas-phase water molecules. *J. Chem. Phys.* **136**, 144311 (2012).

9. Zhovtobriukh, I., Besley, N. A., Fransson, T., Nilsson, A. & Pettersson, L. G. M. Relationship between x-ray emission and absorption spectroscopy and the local h-bond environment in water. *The Journal of Chemical Physics* **148**, 144507 (2018).

10. Smith, J. D. *et al.* Energetics of Hydrogen Bond Network Rearrangements in Liquid Water. *Science* **851**, 851–854 (2004).

11. Smith, J. D. *et al.* Probing the Local Structure of Liquid Water by X-ray Absorption Spectroscopy . *J. Phys. Chem. B* **110**, 20038–20045 (2006).

12. Santra, B., DiStasio, R. A., Martelli, F. & Car, R. Local structure analysis inab initioliquid water. *Molecular Physics* **113**, 2829–2841 (2015).

13. Ghiringhelli, G. *et al.* Saxes, a high resolution spectrometer for resonant x-ray emission in the 4001600ev energy range. *Rev. Sci. Instrum.* **77**, 113108 (2006).

14. Vaz da Cruz, V. *et al.* A study of the water molecule using frequency control over nuclear dynamics in resonant x-ray scattering. *Phys. Chem. Chem. Phys.* **19**, 19573–19589 (2017).

15. Ertan, E. *et al.* Ultrafast dissociation features in rixs spectra of the water molecule. *Phys. Chem. Chem. Phys.* **20**, 14384–14397 (2018).

16. Wernet, P. *et al.* The structure of the first coordination shell in liquid water. *Science* **304**, 995–999 (2004).

17. Myneni, S. *et al.* Spectroscopic probing of local hydrogen-bonding structures in liquid water. *J. Phys. Condens. Matter* **14**, L213–L219 (2002).

18. Prendergast, D. & Galli, G. X-ray absorption spectra of water from first principles calculations. *Phys. Rev. Lett.* **96**, 215502 (2006).

19. Sun, Z. *et al.* X-ray absorption of liquid water by advanced ab initio methods. *Phys. Rev. B* **96**, 104202 (2017).

20. Iannuzzi, M. & Hutter, J. Inner-shell spectroscopy by the gaussian and augmented plane wave method. *Phys. Chem. Chem. Phys.* **9**, 1599–1610 (2007).

21. Fortin, F.-A., De Rainville, F.-M., Gardner, M.-A., Parizeau, M. & Gagné, C. DEAP: Evolutionary algorithms made easy. *J. Mach. Learn. Res.* **13**, 2171–2175 (2012).

22. Gel'mukhanov, F. & Ågren, H. Resonant X-ray Raman Scattering. *Phys. Rep.* **312**, 87–330 (1999).

Acknowledgements This work was supported by the Swedish Research Council (VR) and the Knut and Alice Wallenberg foundation (Grant No. KAW-2013.0020); FG and VK acknowledge the Russian Science Foundation (project 16-12-10109); MD and TS acknowledge funding from the Swiss National Science Foundation within the D-A-CH programme (SNSF Research Grant 200021L 141325). S.E. and A.F. acknowledge funding from the ERC-ADG-2014 - Advanced Investigator Grant - n° 669531 EDAX under the Horizon 2020 EU Framework, Programme for Research and Innovation. M. O. and A. F. acknowledge partial funding by the Helmholtz Virtual Institute VI419 "Dynamic Pathways in Multidimensional Landscapes". The calculations were performed on resources provided by the Swedish National Infrastructure for Computing (SNIC).

Competing Interests The authors declare no competing interests.

Author contributiuons The experiment was designed and developed by S.E., A.P., J.N., M.F., M.D., B.K., T.S., X.L., D.M., R.M.J. and A.F. The samples were bought from Sigma Aldrich. The experiments were performed by J.N., S.E., R. M. J., M. F., and A. P. The data were analysed and interpreted by V.V.C., J.N., A.P., F.G., M.O., V.K., R.C.C., and A.F. The *ab initio* MD, potential energy calculations and quantum wave packet simulations were performed by V.V.C., M.O., M.I., and E.E. The manuscript was written by V.V.C., F.G., and M.O. All authors commented on the manuscript. The project was led by M.O., V.V.C. and A.F.

Correspondence Correspondence and requests for materials should be addressed to V.V.C. and M.O.

Methods

Experiment. The experimental RIXS spectra presented here were measured with the SAXES spectrometer[13] at the RIXS end station of the ADRESS beam line[23] at the Swiss Light Source. We utilised a flow-cell separating the sample from the vacuum by a Si_3N_4 window of 150 nm thickness with a $\sim$10 nm Au coating. The energy calibration was based on the O_2 spectrum[24]. Due to breakdown of the windows in irradiation, the cell was moved every 10 min. To avoid errors from this procedure, the event lists of these individual scans were shifted to same energy scale by using a fit to the elastic line before joining them for a single one for further data processing. The experimental RIXS spectra shown here were measured for the photon energy tuned in the pre-edge peak ($\omega \approx 535$ eV for liquid water and $\omega \approx 534.1$ eV for gas phase water, respectively). The resonantly scattered photons were detected at a 90° angle from the incoming photons with a combined experimental resolution of 40 meV for liquid water and 75 meV for gas phase water, respectively.

Quantum-classical theory of RIXS. The simulations of the RIXS spectrum of liquid water were carried out employing a two level classical-quantum approach. First, the liquid phase was simulated using *ab-initio* molecular dynamics MD of a 64-molecule system subject to periodic boundary conditions. On the second step, cuts through the ground and core-excited potential energy surfaces along both OH bonds were sampled over all 64 water molecules in a snapshot from the MD simulation. These potentials energy curves (PEC) were used in quantum simulations of the partial RIXS cross sections $\sigma_k(\omega, \omega')$ for each k-th molecule in the configuration. The total RIXS cross-section of the scattering from the ground state (0) via the core-excited state (c) to the final electronic

state (f) was calculated as the sum over these partial contributions

$$\sigma(\omega', \omega) = \sum_{k=1}^{64} \sigma_k(\omega, \omega'). \tag{3}$$

In order to compute the vibrationally resolved RIXS, we use a quantum description of the OH vibrations in liquid water. The Hamiltonian, in valence coordinates, on the electronic state $i = 0, c, f$ for each molecule

$$h_k^i = -\frac{1}{2\mu}\left(\partial_{R_1}^2 + \partial_{R_2}^2\right) - \frac{\cos\theta_0}{m_O}\partial_{R_1R_2}^2 + V_k^i(R_1, R_2), \tag{4}$$

is approximated by assuming an independent bond approximation, $V_k^i(R_1, R_2) \approx V_k^i(R_1, R_2^{eq}) + V_k^i(R_1^{eq}, R_2) - V_k^i(R_1^{eq}, R_2^{eq})$, with a frozen local environment, where R_1 and R_2 are the OH bond lengths of the k-th molecule; the label (eq) marks the equilibrium position; $\mu = m_H m_O/(m_H + m_O)$ where m_H and m_O are the masses of the hydrogen and oxygen atoms; θ_0 is the equilibrium $\angle$HOH angle; and V_k^i is the molecular potential along a OH bond of the k-th molecule in the configuration on the electronic state $|i\rangle$. The ground state vibrational spectrum of molecule k is then given by the time independent Schrödinger equation $h_k^0|\phi_{n_1,n_2}\rangle = \epsilon_{n_1,n_2}|\phi_{n_1,n_2}\rangle$, where ϕ_{n_1,n_2} is the 2D vibrational eigenstate with the respective energy ϵ_{n_1,n_2}.

The single molecule cross-sections were computed using the quantum wave packet formal-

ism[3,14], as the half-Fourier transform of the auto-correlation function

$$\sigma_k(\omega,\omega') = \frac{|\mathrm{d}^k_{f,c}\mathrm{d}^k_{c,0}|^2}{\pi} \times \mathrm{Re}\int_0^\infty dt\ e^{\imath(\omega-\omega'-\omega^k_{f0}+\epsilon^k_{0,0}+\imath\Gamma)t}\langle\Psi_k(0)|\Psi_k(t)\rangle, \tag{5}$$

defined by the nuclear wave packets

$$|\Psi_k(0)\rangle = \int_0^\infty dt\ e^{\imath(\omega-\omega^k_{i0}+\epsilon^k_{0,0}+\imath\Gamma)t}|\psi_k(t)\rangle, \tag{6}$$
$$|\psi_k(t)\rangle = e^{-\imath h^c_k t}|\phi^k_{0,0}\rangle, \quad |\Psi_k(t)\rangle = e^{-ih^f_k t}|\Psi_k(0)\rangle, .$$

Here $\mathrm{d}^k_{i,j}$ is the transition dipole moment, at the equilibrium geometry, between the electronic states i and j for the k-th molecule. In liquid phase, the scattered X-ray photons are very likely to be reabsorbed by nearby molecules. We account for this effect by carrying out a self-absorption correction in the same fashion as in previous work[14,25].

In parallel with the RIXS cross section we use also the density of vibrational states

$$\rho_n(\epsilon) = \sum_{k=1}^{64}\sum_{n_1+n_2=n}\Phi(\epsilon-\epsilon^k_{n_1,n_2}+\epsilon^k_{0,0}), \tag{7}$$

where $\Phi(x) = \exp(-x^2/\delta^2)/\delta\sqrt{\pi}$, $\delta = 0.01$ eV, n_1 and n_2 are the vibrational quantum numbers for the stretching modes along the OH bonds in the k-th water molecule.

To reconstruct the liquid spectrum $\sigma_{\mathrm{liquid}}(\omega',\omega)$ from the one in gas phase we convolute the

experimental gas-phase spectrum $\sigma_{\rm gas}(\omega', \omega)$ with the distribution function $\rho(\omega'_1 - \omega')$

$$\sigma_{\rm liquid}(\omega', \omega) \approx \int_{-\infty}^{\infty} \sigma_{\rm gas}(\omega'_1, \omega)\rho(\omega'_1 - \omega')d\omega', \tag{8}$$

where $\rho(\omega'_1 - \omega') = \exp\left(-\frac{4\ln 2(\omega'_1 - \omega')^2}{\gamma^2}\right)$. The employed structural inhomogeneous broadening $\gamma(\mathrm{FWHM}) = 0.35eV$ is in reasonable agreement with the 0.45 eV value obtained using molecular dynamics simulations[9].

Computational details. For consistency of analysis, the wave-packet simulations were performed on the same configuration as our previously classical spectrum simulations[6,7] of liquid water, which was obtained from *ab initio* MD simulations with periodic boundary conditions in the CPMD program[26] using the gradient-corrected BLYP functional[27,28] (See Ref.[6,7] for further details).

The dissociative $4a_1$ band was modelled with the excited core-hole method (XCH)[18], based on density functional theory (DFT) in which the lowest lying core-excited state forms the pre-edge peak in both gas phase and liquid water. This level of theory has already been shown to accurately reproduce the pre-edge feature of XAS[7,18] of liquid water which is the main focus of this article. The molecular potentials of and transition dipole moment between the ground state and the lowest O1s core-excited state were computed for each one of the 64 molecules in the sampled configuration. These unrestricted all-electron DFT calculations were performed using the GAPW method in CP2K[20,29,30], employing the BLYP functional[27,28], Ahlrichs-def2-QZVP basis sets[31] and a plane wave cut-off of 300 Ry for the soft part of the density.

Extraction of confidence interval for OH potentials using a genetic algorithm. The potential reconstruction procedure was based on a genetic algorithm (GA) and implemented with the help of the deap python library[21]. The individuals were chosen to be a set of parameters which define the model potential along the OH bond. To obtain the confidence interval for the OH potentials, from the experimental RIXS data, we fitted the parameters (B, β, α, D) of the modified Morse potential

$$V(R) = V_M(R) + Be^{\beta R}, \quad V_M(R) = D\left(1 - e^{\alpha R}\right)^2, \tag{9}$$

using the GA[21] to search for potentials that satisfy the constraints defined by Eqs. (2) and (3) of the main text and described in the surrounding text.

A random initial population (distribution of potentials) is then generated at the initial step and the evolutionary operations are applied to the population until convergence is reached as it is illustrated in Extended Data Fig. 1. The fitness criterion of our GA was based on the concept of a "vibrational eigenvalue distribution", by which we consider whether a given eigenvalue lies within the width of a given peak $\Delta\varepsilon_m$ in the RIXS spectrum (Extended Data Fig. 2), we consider the first 6 peaks (m=1,$\cdots$, 6) of the experimental RIXS spectrum (which are the most relevant according to our analysis).

Proof of principle. To verify the suggested reconstruction technique it is natural to apply it to the theoretical RIXS spectrum and to compare the obtained potentials with the original ones used to compute RIXS. The results of this test calculations depicted in Extended Data Fig. 3 shows a good agreement between the extracted confidence interval and true distribution of the OH potentials.

Apparently, the method should not give exactly the same potential distributions as the input ones. This leads to some small differences between the discussed distributions.

Local structure classification. Even though we recognise that hydrogen bonding is not universally defined[10–12,32–36], we employ a definition based on geometrical criteria[16,33] In our article we use a geometrical classification of the HB (Extended Data Fig. 4) which is similar to ref.[16]. The set of structures which satisfy the constrain

$$R_{OO} < 3.3 \text{ Å}, \quad \Theta < 30^{\circ} \tag{10}$$

only for one OH bond we refer to as $D1$ (single donor) structures while the rest of the structures with both OH bonds forming HBs are referred to as $D2$ (double donor) structures.

It is has been suggested that excitation at the pre-edge region of liquid water leads to the selection of OH bonds with a broken HB[16,17,37], this motivates us to understand the role that this subset of structures alone plays in the formation of the RIXS spectrum of liquid water.

Role of the method used for the transition dipole moment calculations on the relative contribution of D1 and D2 structures. There is a widely discussed problem of extraction of local structure information from RIXS measurements of liquids. Within the used MD simulations we obtained a proportion of 20% D1 structure and 80% D2 structures using the geometrical constraint introduced in the previous section. To check whether our combined theoretical/experimental analysis of RIXS can shed light on the relative contribution of these structures, we performed simulation of the RIXS profile for excitation at the pre-edge region, related to the dissociative core-excited state,

of the studied configuration using different techniques for computing transition dipole moments. Apparently, the relative contributions of D1 and D2 structures are very sensitive to the model used to compute the transition dipole moments.

To show sharply this problem let us imagine that the transition dipole moment associated with D1 structures is much bigger than the ones for D2 structures, in this case we would arise to the erroneous conclusion that D1 structures dominate liquid water, when in fact it would only mean that RIXS would not "see" D2 structures. One should mention that similar questions are raised in XAS studies of liquid water[7,16,17,38]. Extended Data Fig. 5 displays this problem more accurately. We have used three techniques of calculation one of which exaggerates the transition dipole moment of D1 structures, namely the half core-hole (HCH) method[20], and two which have a more balanced distribution, the full core-hole (FCH)[20] and XCH methods. These three different techniques give the following relative contribution D1-D2 to the total RIXS profile: HCH 86%-14%, FCH 53%-47% and XCH 57%-43%. We see that 86% of D1 contribution in RIXS does not reflect the actual 20% fraction of D1 structures in the configuration obtained from the MD simulations. In spite of that, Extended Data Fig. 5 shows that the total RIXS spectra for these three DFT-based techniques is almost the same. Thus we can not draw definite conclusions about the overall local structure configuration of liquid water from RIXS data, but we can clearly conclude that the configurations, which are actually probed at the XAS pre-edge, have a broad distribution of ground potential shapes.

Role of the single bond approximation on RIXS . Now let us turn our attention to the single bond approximation usually used in analysis of RIXS of liquid water. In earlier studies[1,2], it is suggested that the vibrational progression seen in RIXS may be understood simply in terms of a

Morse potential along a single OH bond, namely the one with a broken HB, which exists only in the D1 subset. As one can see from Extended Data Fig. 6a this approximation $\sigma_{D1}^{\mathrm{sb}}$ does not match with the strict theoretical RIXS profile, σ.

The single bond approximation which include all OH bonds (broken and intact) as well as all structures D1 and D2 gives even worse agreement (Extended Data Fig. 6b). The reason for this discrepancy is that the single bond approximation neglects that the both OH bonds are excited in scattering process coherently (this is seen in Fig. 2a and is accounted in strict RIXS profile) resulting the manifold of mixed excitations.

23. Strocov, V. N. *et al.* High-resolution soft X-ray beamline ADRESS at the Swiss Light Source for resonant inelastic X-ray scattering and angle-resolved photoelectron spectroscopies. *J. Synchrotron Radiat.* **17**, 631–643 (2010).

24. Hennies, F. *et al.* Resonant inelastic scattering spectra of free molecules with vibrational resolution. *Phys. Rev. Lett.* **104**, 193002 (2010).

25. Sun, Y.-P. *et al.* Intramolecular Soft Modes and Intermolecular Interactions in Liquid Acetone. *Phys. Rev. B* **84**, 132202 (2011).

26. CPMD. Copyright IBM Corporation 1990–2012; MPI für Festkörperforschung: Stuttgart, Germany, 1997–2001. www.cpmd.org.

27. Becke, A. D. Density-functional exchange-energy approximation with correct asymptotic behavior. *Phys. Rev. A* **38**, 3098–3100 (1988).

318 28. Lee, C., Yang, W. & Parr, R. G. Development of the colle-salvetti correlation-energy formula
319 into a functional of the electron density. *Phys. Rev. B* **37**, 785–789 (1988).

320 29. CP2K. Version 2.6 the CP2K developers group. http://www.cp2k.org (2014).

321 30. Hutter, J., Iannuzzi, M., Schiffmann, F. & VandeVondele, J. cp2k: atomistic simulations of
322 condensed matter systems. *Wiley Interdiscip. Rev. Comput. Mol. Sci.* **4**, 15–25 (2014).

323 31. Weigend, F. & Ahlrichs, R. Balanced basis sets of split valence, triple zeta valence and
324 quadruple zeta valence quality for H to Rn: design and assessment of accuracy. *Phys. Chem.*
325 *Chem. Phy.* **7**, 3297–3305 (2005).

326 32. Auer, B., Kumar, R., Schmidt, J. R. & Skinner, J. L. Hydrogen bonding and raman, ir, and
327 2d-ir spectroscopy of dilute hod in liquid d2o. *Proc. Natl. Acad. Sci. U.S.A.* **104**, 14215–14220
328 (2007).

329 33. Kumar, R., Schmidt, J. R. & Skinner, J. L. Hydrogen bonding definitions and dynamics in
330 liquid water. *J. Chem. Phys.* **126**, 204107 (2007).

331 34. Henchman, R. H. Waters dual nature and its continuously changing hydrogen bonds. *Journal*
332 *of Physics: Condensed Matter* **28**, 384001 (2016).

333 35. Shiratani, E. & Sasai, M. Growth and collapse of structural patterns in the hydrogen bond
334 network in liquid water. *J. Chem. Phys.* **104**, 7671–7680 (1996).

335 36. Appignanesi, G. A., Rodriguez Fris, J. A. & Sciortino, F. Evidence of a two-state picture for

supercooled water and its connections with glassy dynamics. *The European Physical Journal E* **29**, 305–310 (2009).

37. Harada, Y. *et al.* Probing the oh stretch in different local environments in liquid water. *J. Phys. Chem. Lett.* **8**, 5487–5491 (2017).

38. Chen, W., Wu, X. & Car, R. X-ray absorption signatures of the molecular environment in water and ice. *Phys. Rev. Lett.* **105**, 017802 (2010).

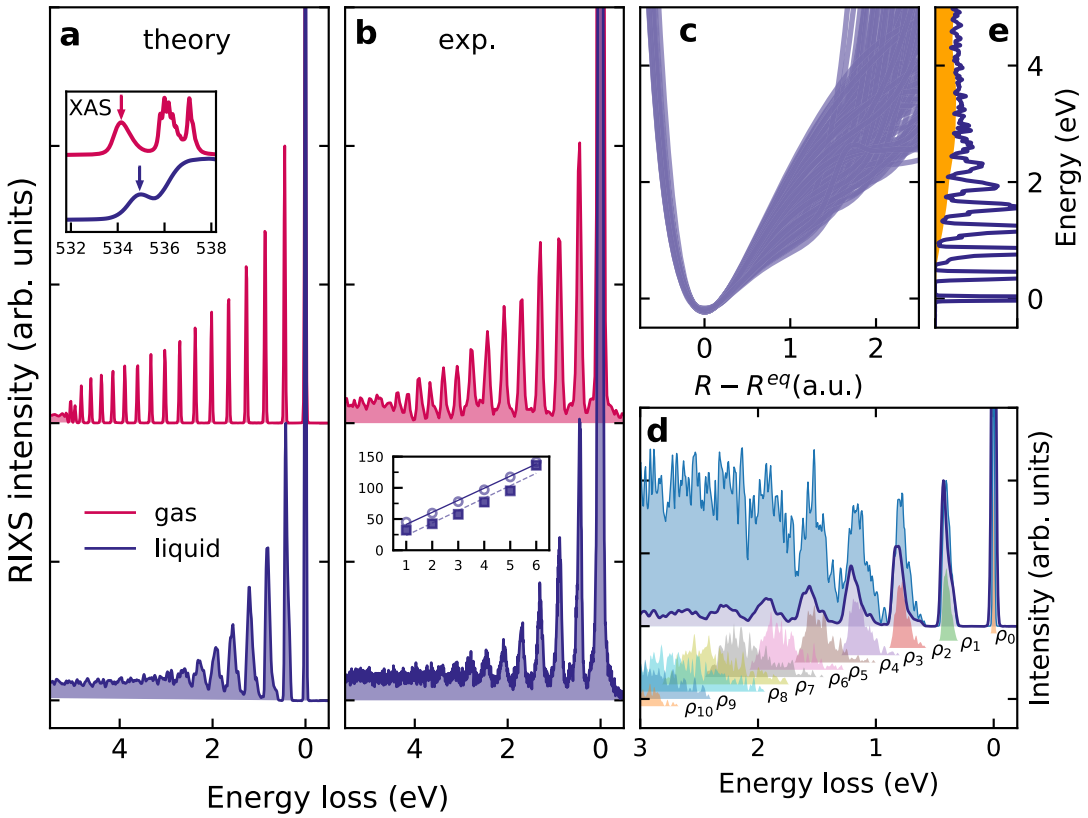

Figure 1: **RIXS spectra of water in gas and liquid phases under $4a_1$ and pre-edge core excitations, respectively**. a) Theoretical RIXS spectra of gas phase and liquid water vs the energy loss ($\omega - \omega'$). The insert shows energy of resonant excitation in the XAS of free water molecules and liquid water. b) Experimental RIXS spectra of gas phase and liquid water. The insert compares experimental (circles) and theoretical (squares) peak widths in meV as a function of the peak number m. c) *ab initio* potential energy curves along the OH bonds for each of the 64 sampled water molecules in liquid water d) Partial densities of the vibrational states ρ_n (see eq. (7)) and the total density of states $\rho = \sum_n \rho_n$ together with the RIXS profile σ. e) Overlap of the partial RIXS cross sections results in the formation of a background shown in yellow (Compare with the overlap of the partial densities of vibrational states (d))

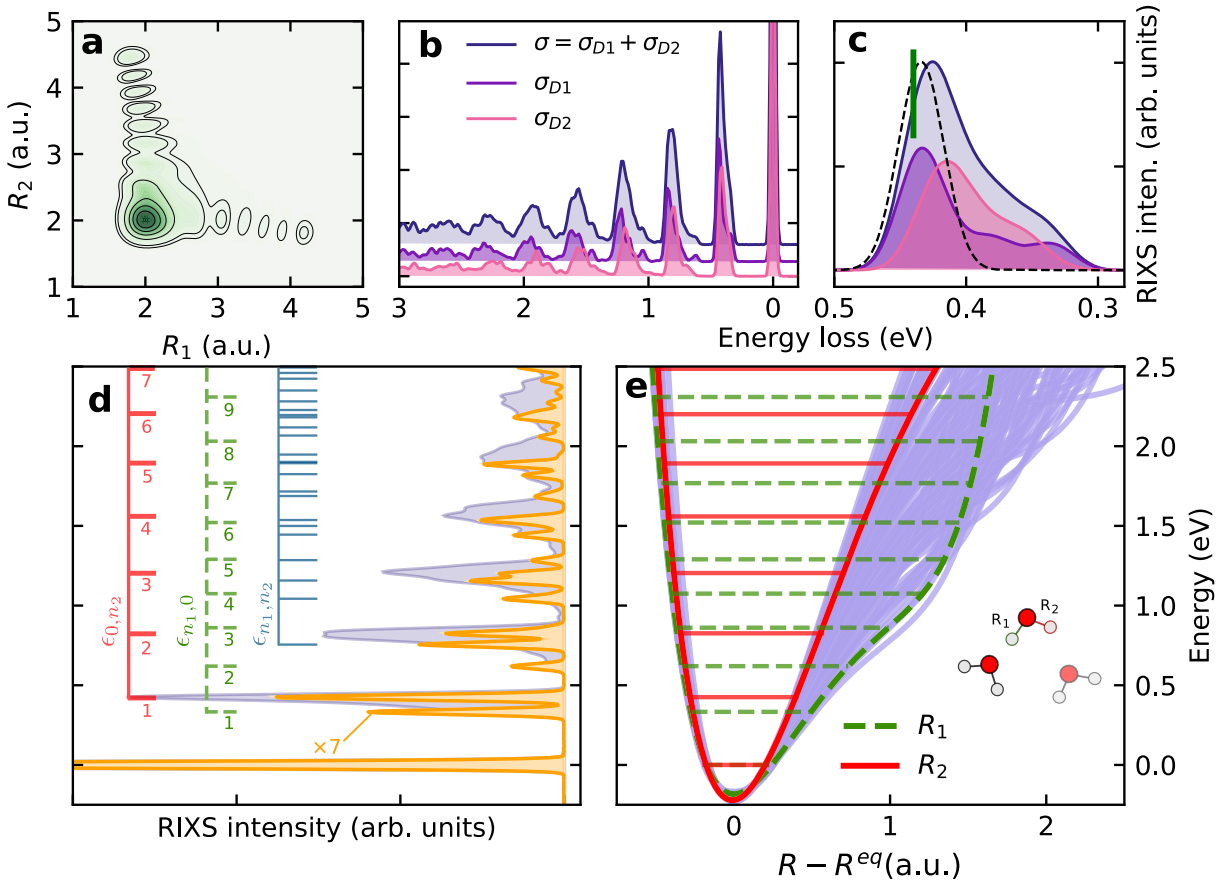

Figure 2: **Role of coherent excitation of both OH bonds**. a) The nuclear core-excited wave packet squared shows coherent excitation of both OH bonds in a D2 configuration. b) Partial RIXS cross sections σ_{D1} and σ_{D2}. c) Partial contributions to the RIXS peak $m = 1$. The dashed curve shows the result from the single bond approximation $\sigma^{sb}_{D_1}$ simulated including only the single OH stretches with a broken HB. The vertical green bar shows the theoretical peak position of the RIXS in gas phase water. Current DFT(BLYP) description gives a slight red-shift of the peaks relative to experiment and to high-level calculations[3,14,15]. d) Total RIXS profile(blue) and assignment of RIXS spectrum (yellow) of a single asymmetric $D1$ structure. e) All OH potentials(blue) of the sampled configurations. Solid red and dashed green curves show the steep (no HB) and shallow (HB) OH potentials of the $D1$ structure in (d). Subsets of eigenvalues $\epsilon_{n_1,0}$(solid red) and ϵ_{0,n_2}(dashed green) in panels (d) and (e) assign the single bond excitations associated with potentials of corresponding color while the subset ϵ_{n_1,n_2} (blue) displays the mixed excitation overtones.

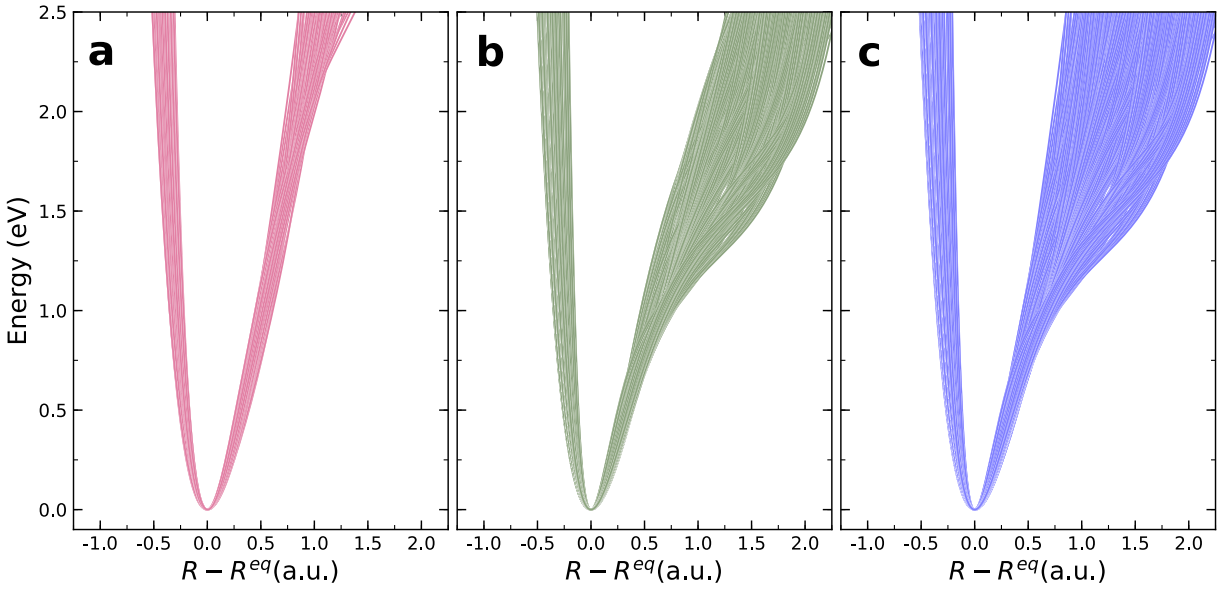

Figure 3: **Confidence intervals for OH potentials extracted from the experimental RIXS spectrum (Fig. 1 (b)) using a genetic algorithm.** a) confidence interval for the PECs in the case of weak HB, corresponding to the constraint in eq. (1); b) confidence interval for PECs of OH bonds in the case of stronger HB (eq. (2)). c) The whole set of the PECs obtained by combining a) and b).

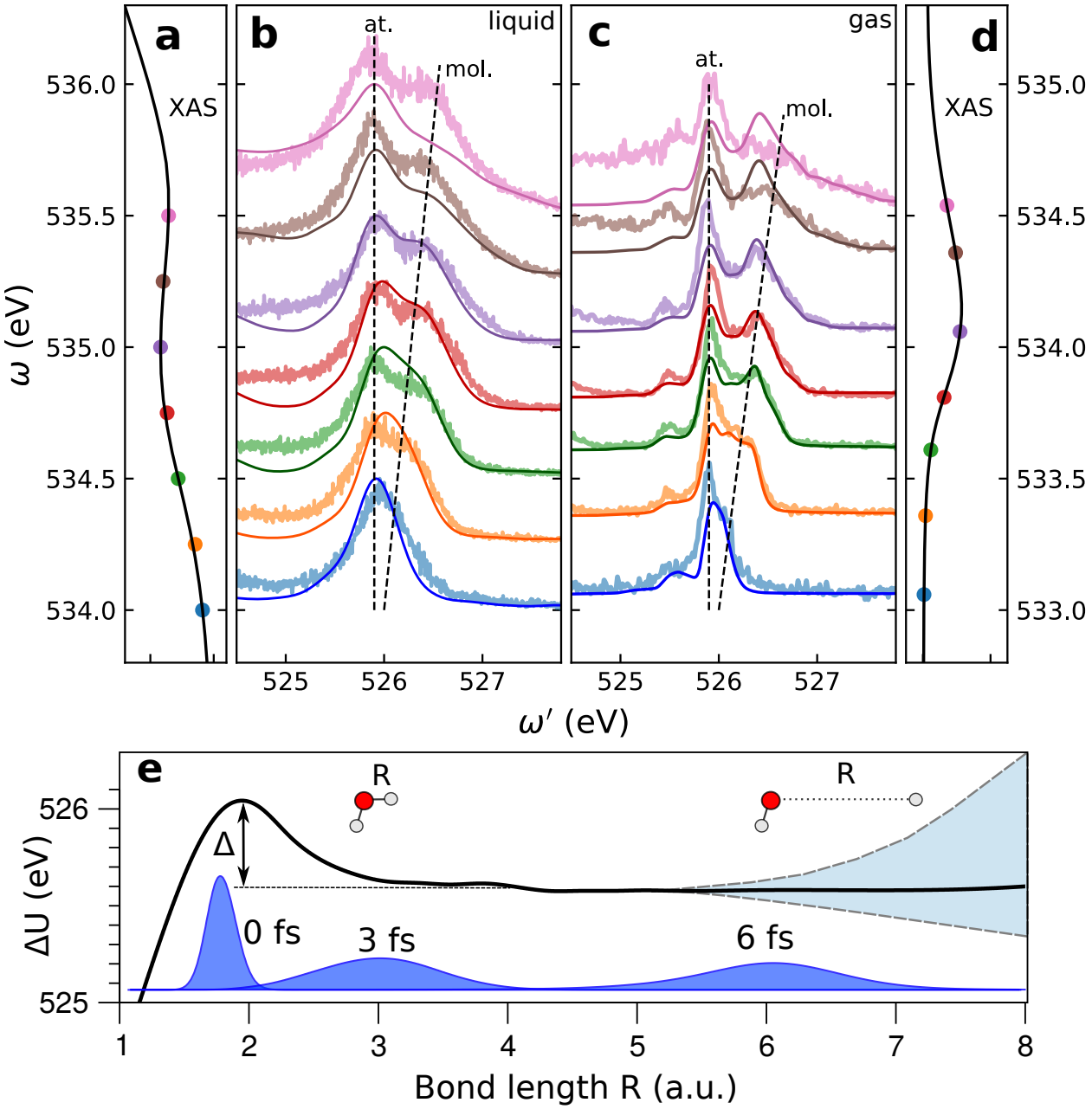

Figure 4: **Dynamical origin of the splitting of the $1b_1$ peak.** Comparison of the dispersion of the split components in experimental RIXS spectra of liquid (b) and gas phase water (c) at the pre-edge region. The panels a) and d) indicating the corresponding excitation energies in the XAS pre-edge region for liquid and gas phase water. Panel c) include theoretical gas-phase RIXS spectra (solid lines). Solid lines in the panel b) show liquid spectra $\sigma_{\rm liquid}(\omega', \omega)$ calculated by convolution of the experimental gas phase spectra $\sigma_{\rm gas}(\omega', \omega)$ with the structure function $\rho(\omega'_1 - \omega')$ (see eq.(8)) with FWHM=0.35 eV. Both liquid b) and gas phase c) spectra display a nondispersive component (pseudo-atomic peak) and a molecular band following the Raman dispersion law. Panel e) illustrates schematically how the pseudo-atomic peak is formed near ($R = 3$ a.u.) equilibrium as the PECs of core-excited $U_c(R)$ and final $U_f(R)$ states become almost parallel: $\Delta U = U_c(R) - U_f(R) \approx \text{const}$. The parameter $\Delta \approx 0.45$ eV is the splitting between molecular and pseudo-atomic peaks on top of the XAS resonance.

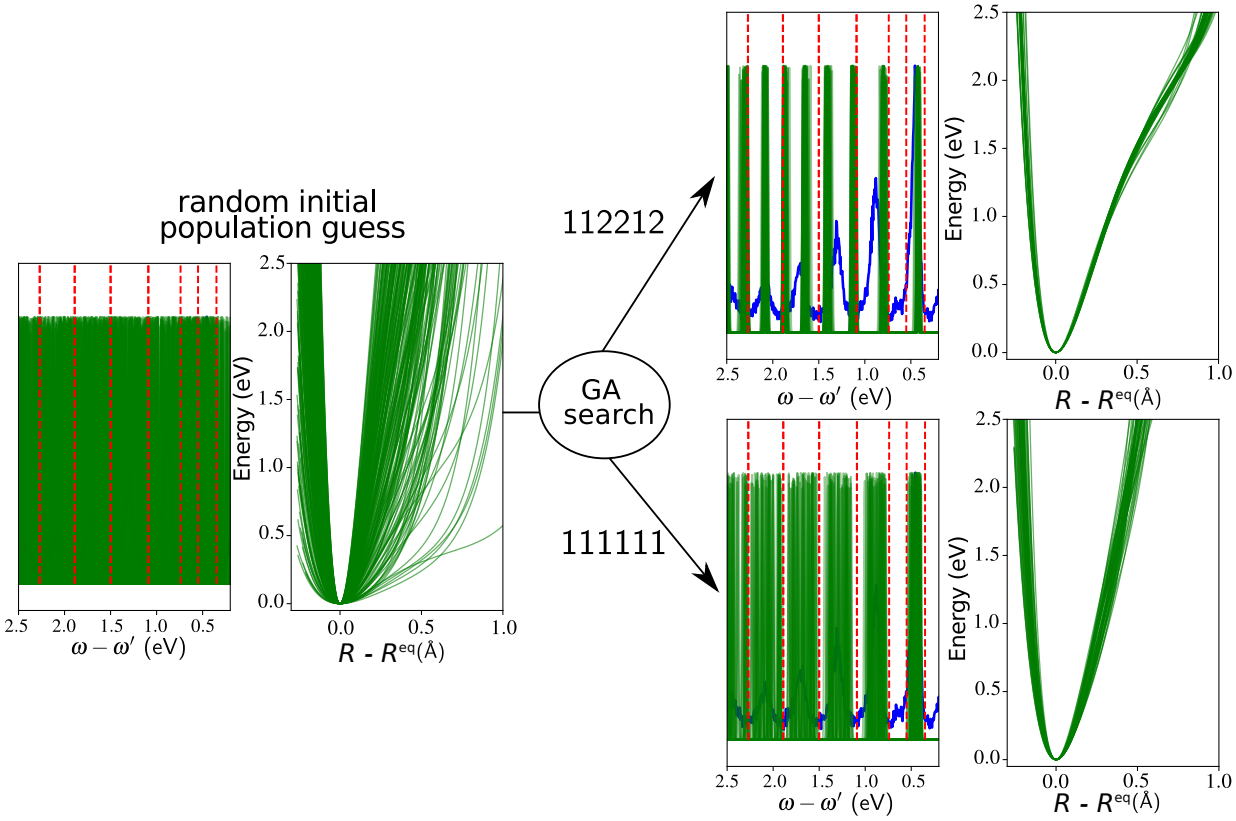

Extended Data Fig. 1: **Explanation of the reconstruction of the potentials through the genetic algorithm (GA)**. Left panel shows that randomly generated initial distribution of the potentials (without any constraints) leads to a quasi-continuum spectrum. Right panel displays the distribution of the OH potentials selected by GA for two individual constraints: (111111) and (112212), contained in eq.(2) and (3) of main text, respectively.

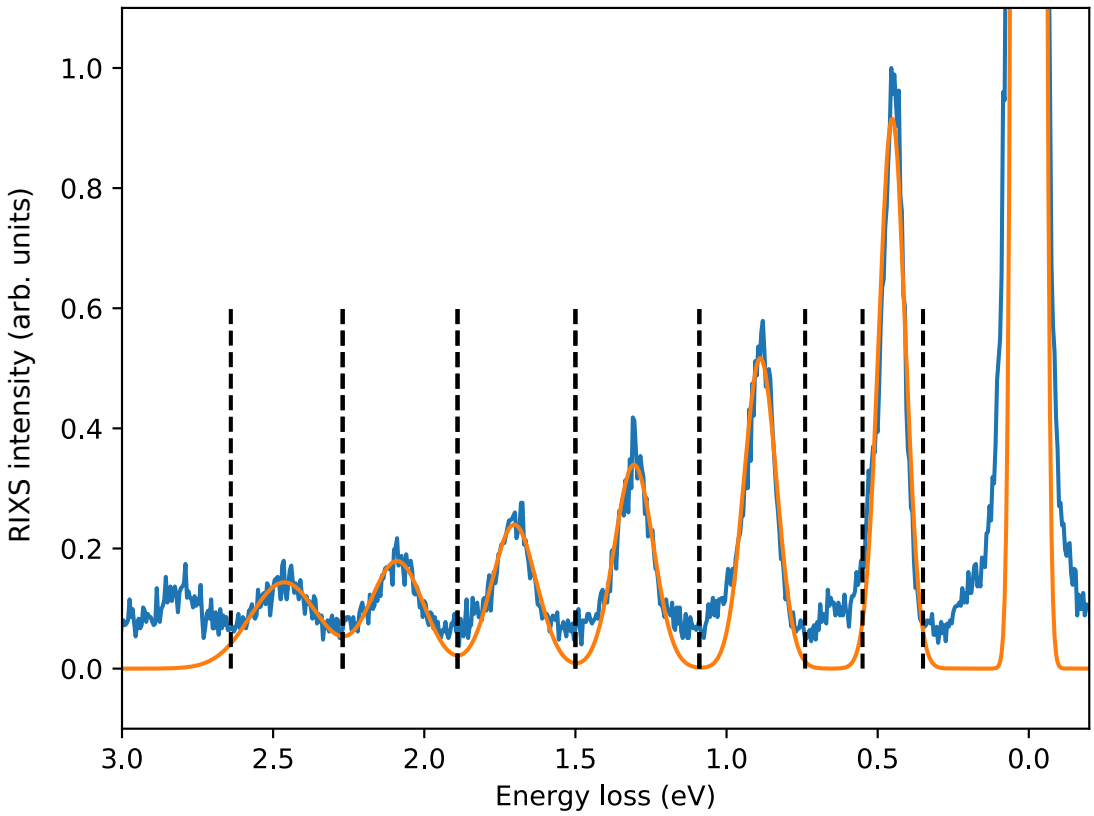

Extended Data Fig. 2: **Division of the spectrum into intervals,** $\Delta\epsilon_m$. Experimental RIXS spectrum and its Gaussian fit are shown by blue and orange, respectively. The division into intervals was performed using the Gaussian fit.

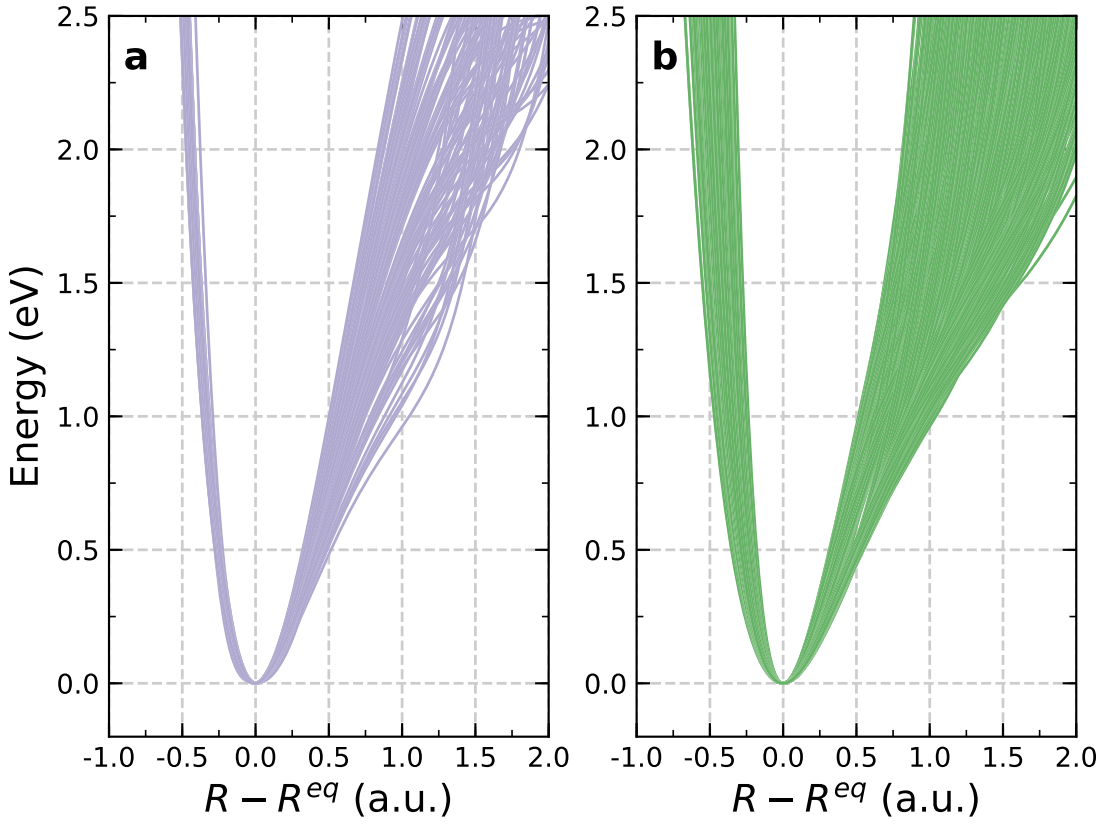

Extended Data Fig. 3: **Validation of the confidence interval extraction**. a) Distribution of the *ab initio* potentials. b) Confidence interval reconstructed from the theoretical RIXS spectrum based on the potentials shown in the panel (a).

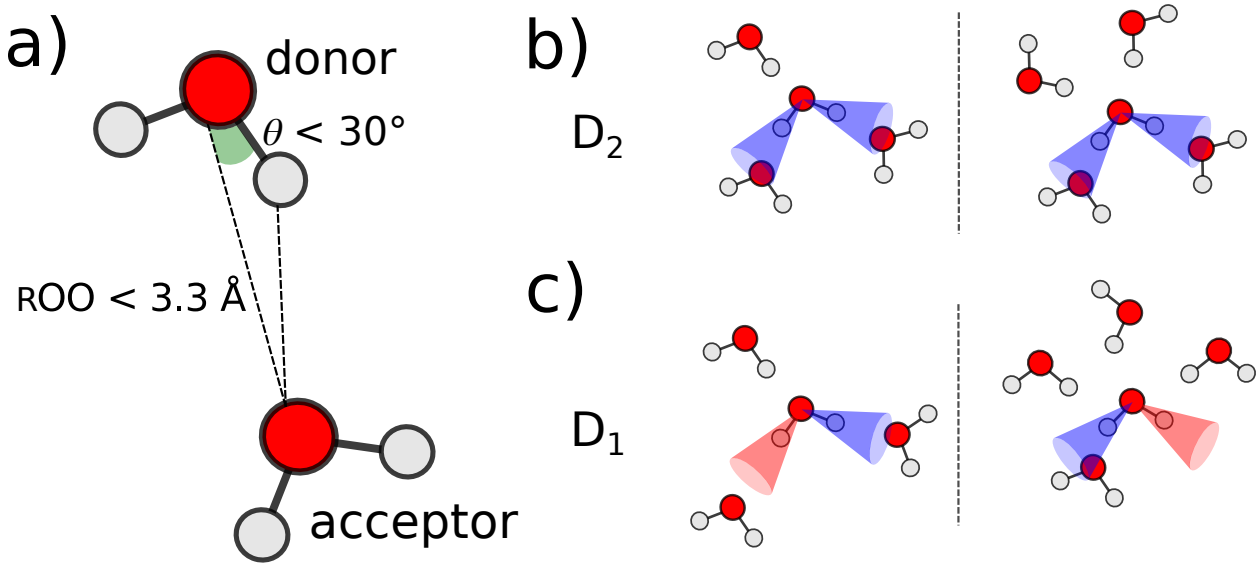

Extended Data Fig. 4: **Hydrogen bond classification**. a) schematic depiction of the local HB classification employed. b) and c) Illustration of possible $D2$ and $D1$ structures, respectively.

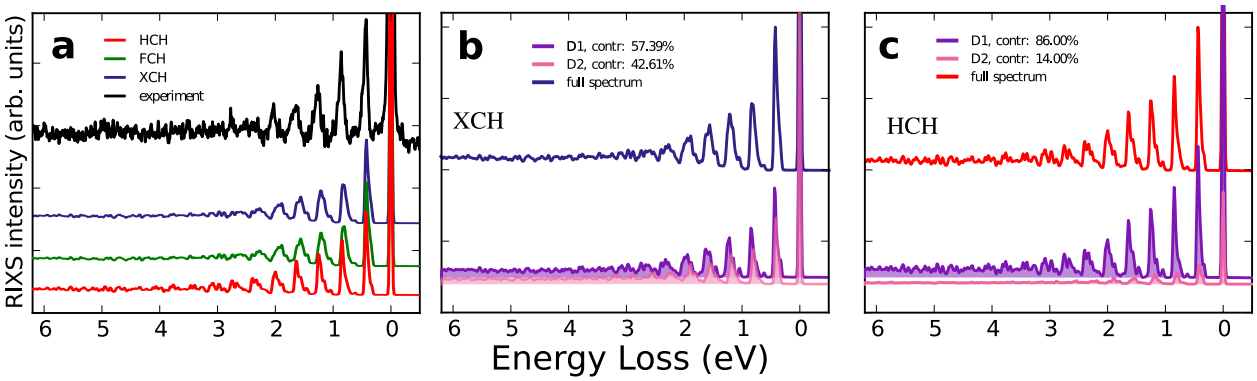

Extended Data Fig. 5: **The role of the method of calculations of transition dipole moment on the RIXS profile.** a) Comparison between the total RIXS profile and the theoretical ones computed using transition dipole moments yielded by the HCH, FCH and XCH methods[20]. Total and partial theoretical RIXS cross-sections for different local structure subsets computed with XCH (b) and HCH (c) dipoles. The percentages show the contributions of D1 and D2 structures in the total RIXS profile. Different quantum chemical methods result in different numbers because they give different transition dipole moments. We omit here the FCH partial analysis because its almost identical to the XCH case shown in panel (b).

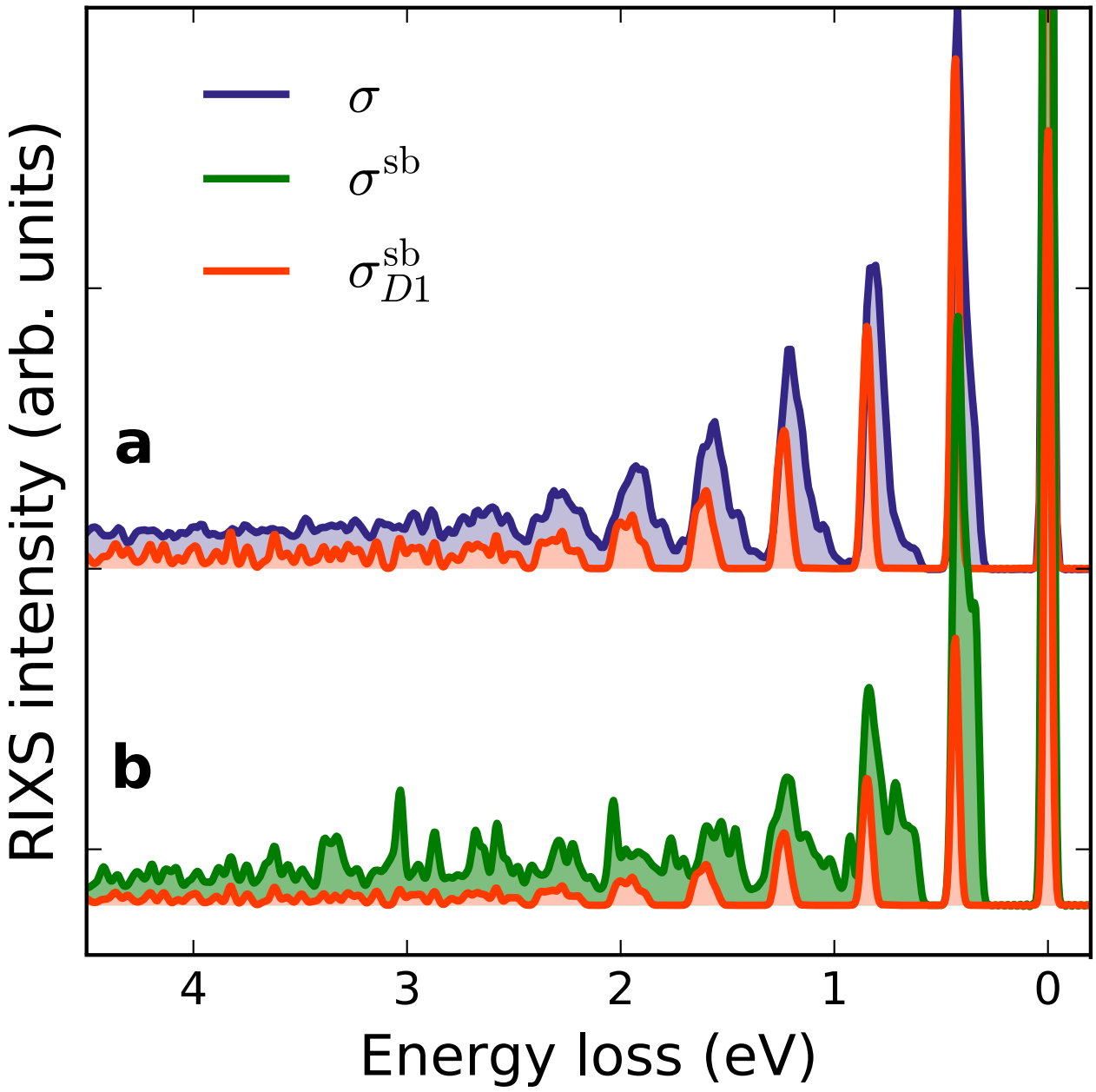

Extended Data Fig. 6: **Non-validity of the single-bond model**. (a)(comparison of total theoretical RIXS spectrum σ (dark blue) and the RIXS composed only the non-hydrogen bonded potentials σ^{sb}_{D1} (red) for all D1 structures (single bond calculations). (b) RIXS spectra considering a single bond model for all OH bonds and all structures in the configuration σ^{sb} (green) alongside σ^{sb}_{D1}.